



Research article

Repurposing of US-FDA-approved drugs as negative modulators of ubiquitin specific protease-7 (USP7)

Seema Zadi^a, Sumaira Javaid^{a,*}, Atia-tul-Wahab^a, Humaira Zafar^a, Muhammad Awais^a, Innokentiy Maslennikov^d, M. Iqbal Choudhary^{a,b,c,**}^a Dr. Panjwani Center for Molecular Medicine and Drug Research, International Center of Chemical and Biological Sciences, University of Karachi, Karachi, 75270, Pakistan^b H. E. J. Research Institute of Chemistry, International Center for Chemical and Biological Sciences, University of Karachi, Karachi, 75270, Pakistan^c Department of Biochemistry, Faculty of Sciences, King Abdulaziz University, Jeddah, 22252, Saudi Arabia^d School of Pharmacy, Chapman University Irvine, CA, 92866, USA

ARTICLE INFO

Keywords:

Drug repurposing
Deubiquitinase
USP7
Anti-cancer agents
STD-NMR
Gene expression analysis
Oxybutynin
Ketotifen
Pantoprazole sodium
Escitalopram

ABSTRACT

Ubiquitin-specific protease7 (USP7) regulates the stability of the p53 tumor suppressor protein and several other proteins critical for tumor cell survival. Aberrant expression of USP7 facilitates human malignancies by altering the activity of proto-oncogenes/proteins, and tumor suppressor genes. Therefore, USP7 is a validated anti-cancer drug target. In this study, a drug repurposing approach was used to identify new hits against the USP7 enzyme. It is one of the most strategic approaches to find new uses for drugs in a cost- and time-effective way. Nuclear Magnetic Resonance-based screening of 172 drugs identified 11 compounds that bind to the catalytic domain of USP7 with dissociation constant (K_d) values in the range of 0.6–1.49 mM. These 11 compounds could thermally destabilize the USP7 enzyme by decreasing its melting temperature up to 9 °C. Molecular docking and simulation studies provided structural insights into the ligand-protein complexes, suggesting that these compounds bind to the putative substrate binding pocket of USP7, and interact with its catalytically important residues. Among the identified 11 hits, compound 6 (oxybutynin), 7 (ketotifen), 10 (pantoprazole sodium), and 11 (escitalopram) also showed anti-cancer activity with an effect on the expression of proto-oncogenes and tumor-suppressor gene at mRNA level in HCT116 cells. The compounds identified in this study can serve as potential leads for further studies.

1. Introduction

Ubiquitination is a post-translational modification that involves the covalent attachment of ubiquitin to lysine residues of the protein destined to be degraded. It is a key component of the ubiquitin-proteasome system (UPS), which plays an important role in several crucial cellular processes [1]. The dysregulation of the UPS in various diseases, including malignancies, inflammation, and neurodegenerative disorders [2,3], has been extensively reported, making USPs a valid target for drug discovery and development. The ubiquitination can be reversed by deubiquitinase enzymes (an integral component of UPS) that remove the ubiquitin from a substrate

* Corresponding author. International Center of Chemical and Biological Sciences, University of Karachi, Karachi-75270, Pakistan.

** Corresponding author. International Center of Chemical and Biological Sciences, University of Karachi, Karachi-75270, Pakistan.

E-mail addresses: sumairajavid17@yahoo.com, sumaira.javed@iccs.edu (S. Javaid), iqbal.choudhary@iccs.edu (M.I. Choudhary).<https://doi.org/10.1016/j.heliyon.2024.e26345>

Received 27 October 2023; Received in revised form 10 February 2024; Accepted 12 February 2024

Available online 23 February 2024

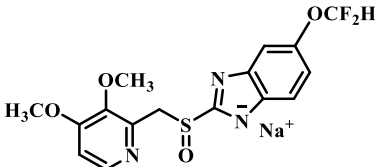
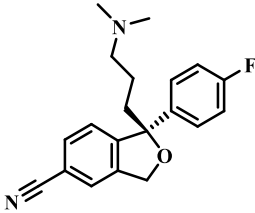
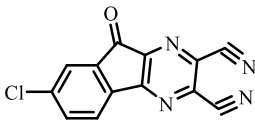
2405-8440/© 2024 The Author(s). Published by Elsevier Ltd. This is an open access article under the CC BY-NC-ND license (<http://creativecommons.org/licenses/by-nc-nd/4.0/>).

Table 1
Compounds identified that interact with catalytic domain of USP7 enzyme.

Drug No.	Drug code/Common Name	Structure	Thermal Shift (Δt_m)	Dissociation constant, K_d (mM)	IC ₅₀ (μ M)
1.	DB 439/Bromfenac Sodium		12.2	0.78 ± 0.53	–
2.	DB 052/Diclofenac Sodium		2.40	0.76 ± 0.56	–
3.	DB134/Ketoprofen)		3.70	0.62 ± 0.56	–
4.	DB 095/Labetalol Hydrochloride		3.95	0.91 ± 0.70	–
5.	DB 272/Orphenadrine		2.30	1.10 ± 0.80	–
6.	DB284/Oxybutynin HCl		2.90	0.66 ± 0.46	36.25 ± 1.03
7.	DB 144/Ketotifen		6.80	1.1 ± 0.88	89 ± 1.55
8.	DB 081/Ticlopidine Hydrochloride		12.91	1.49 ± 1.41	
9.	DB 118/Lamotrigine		6.30	1.0 ± 0.56	

(continued on next page)

Table 1 (continued)

Drug No.	Drug code/Common Name	Structure	Thermal Shift (Δt_m)	Dissociation constant, K_d (mM)	IC ₅₀ (μ M)
10.	DB145/Pantoprazole Sodium		9.30	0.87 ± 0.28	222 ± 0.29
11.	DB 165/Escitalopram		12.30	1.22 ± 1.12	227.6 ± 0.71
12.	Lab standard for USP7 (HBX 41108)		6.20	–	–

protein. The human genome encodes around 100 deubiquitinases; among them, ubiquitin-specific proteases (USPs) form the largest subclass [4]. These USPs are part of a protein cascade that regulates the intracellular protein breakdown, stress response, and cell cycle. The USP enzymes contribute to tumorigenesis by directly or indirectly regulating the levels of several proto-oncogenes, tumor suppressor genes, and proteins, such as MDM2, p53, PTEN, FOXO, etc [5]. Among the USPs, special attention is given to the USP7 enzyme, whose over-expression contributes to several human malignancies by promoting cell proliferation and DNA repair and by inhibiting apoptosis [6,7].

The USP7 enzyme catalyzes the deubiquitination of a proto-oncoprotein MDM2, initiating the ubiquitination of the p53 protein, and subjecting it to proteasomal degradation. This results in reducing the cellular concentration of tumor suppressor protein p53, thereby promoting cancer cell survival. Hence, inhibition of the USP7 activity could keep ubiquitinated MDM2 available for degradation by UPS and, in turn, protect p53 from proteasomal degradation, and help treat various cancers [5].

Several USP7 inhibitors (listed in Table-S1) have been identified against the USP7 enzyme that belongs to the chemical class of pyrazolo[3,4-d] pyrimidin-4-one-piperidine, oxadiazole, sesquiterpene lactone parthenolide, thiophene, amidotetrahydroacridine, quinazolin-4-one derivatives, cyanopyrrolidine, 2-amino-4-ethylpyridin, 4-hydroxypiperidine, *N*-benzylpiperidinol, and thienopyridine (Table-S1). These inhibitors either bind covalently to the enzyme at the catalytic cleft or cause alteration to the catalytic cysteine residue, i.e., Cys223. Some of them also inhibit the enzyme activity by binding to the allosteric site of the enzyme. Some of them progressed to the preclinical stages of development. However, so far, no drug has been approved for clinical use. Severe toxic profile, low potency, and poor specificity and bioavailability of the identified candidates are key limitations that hinder their potential clinical application (5, 6, 8, 9). Therefore, there is a need to identify compounds that could negatively modulate the activity of USP7 and its functions in cancer progression.

Various methods such as; activity-based probes, fluorescence-based methods (Ub-AMC, Ub-Rho, Ub-PLA2), fluorescence resonance energy transfer methods (TR-FRET), SDS-PAGE-Coomassie method, and MALDI-TOF have been used to screen and identify inhibitors for USPs. However, most of them are either very laborious, time-consuming, challenging, and expensive in terms of synthesizing/obtaining the fluorescent substrates or require high technological expertise [8].

In the current study, we deployed biophysical methods, such as STD-NMR and thermal shift assay (also known as differential scanning fluorimetry; DSF) for the identification of the hits against USP-7 enzyme, as these are best suited for on-target binding validation. Based on the nuclear Overhauser effect (NOE) principle, STD-NMR is an excellent technique for identifying ligands with moderate to weak affinity towards a macromolecule. At the same time, thermal shift assay (TSA) was used to assess the ability of compounds to destabilize the USP7-CD.

A drug repurposing approach was employed to identify new inhibitors for modulating the function of USP7. It is an efficient approach to expedite the process of drug discovery and development. It involves the investigation of approved drugs for new therapeutic indications. It is economically feasible, as the cost of developing a repurposed drug is less (\$ 300 million) than the *de novo* drug development, which is over 1 billion dollars. The prior knowledge of the pharmacokinetics, pharmacodynamics, toxicity, and pre-clinical and clinical data for the candidate drug significantly reduces the time required for its development [10]. For this purpose, we evaluated 172 US-FDA-approved drugs against USP7 enzyme *in vitro*, and identified 11 drugs with the potential to interact with the protein, thus modulating its activity (Table-1).

2. Material and methods

Bacterial strain *E. coli* BL21 (DE3) pLysS was purchased from Novagen, Merck (Germany). Tris-HCl, sodium chloride, ampicillin, potassium phosphate monobasic and dibasic, DNase, Dulbecco's Modified Eagle Medium (DMEM), and phenylmethylsulfonyl fluoride (PMSF) were acquired from Sigma (USA). Isopropyl β -D-1-thiogalactopyranoside (IPTG) was purchased from Carbosynth Ltd. (UK), and glycerol, yeast extract, agar, tryptone, lysozyme, and tris(2-carboxyethyl)phosphine (TCEP) were obtained from Biobasic (Canada). Deuterated dimethylsulfoxide (DMSO- d_6), deuterium oxide (D_2O), and tris salt (Tris- d_{11}) were purchased from Armar Chemicals (Switzerland) and Cambridge Isotope Laboratories, Inc. (USA). Primers for genes were acquired from Macrogen, and the SYBER Green PCR master mix and Revert Aid First-strand cDNA synthesis kit were purchased from Thermo Scientific (USA). The fluorescent dye (Sypro orange) was purchased from Invitrogen Life Technology (USA). The plasmid pETNHT-1, encoding the His-tagged catalytic domain of USP7 (residues 208–560), was kindly provided by Prof. Dr. Andrew P. Turnbull, Cancer Research Laboratories, UK. Human colorectal cancer cell line HCT116 was purchased from the American Type Culture Collection (USA), while 3-(4, 5-dimethylthiazol-2-yl)-2, 5-diphenyl tetrazolium bromide (MTT) was obtained from MP Biomedicals (France), 0.25% Trypsin EDTA was purchased from Gibco, Invitrogen (New Zealand), fetal bovine serum was purchased from A & E Scientific (PAA) (USA), whereas 0.4% Trypan Blue solution was purchased from Amersco (USA). Primers of genes GAPDH- MDM2-p53- c-Myc- and USP7 were purchased from Macrogen (South Korea).

2.1. Plasmid transformation, protein expression and purification

The plasmid was transformed and expressed into *E. coli* BL21(DE3) pLysS, following the protocol reported by Turnbull et al., 2017 [11] with some modifications, as described below. The plasmid construct containing the gene of the catalytic domain of USP7 in pETNHT was transformed in the *E. coli* expression strain, i.e., BL21pLyS. For chemical transformation, the glycerol stock of bacterial cells was revived overnight in terrific broth (TB) at 37 °C in a shaking incubator. The cells were made competent using calcium chloride followed by mixing of these cells with the plasmid. The heat shock method was used to transfer the plasmid into the bacterial cell. The heat shock was given at 42 °C for 60 s. The cells were then spread on an LB agar plate containing plasmid-specific antibiotics and incubated overnight at 37 °C. The plate was checked the next day for the appearance of colonies.

Clones were checked for the presence of the gene by colony PCR. DNA sequencing was carried out, to confirm the sequence of the insert into the vector by Macrogen Inc. Transformed cells were then grown in TB at 37 °C until the culture reached an absorbance of 0.6 at 600 nm, after which culture was induced with 1 mM IPTG at 18 °C for 12–16 h. The culture was pellet down at 4500 rpm, and pellets were kept at –80 °C.

For the purification step, the cell pellet was re-suspended in lysis buffer A (25 mM Tris, 300 mM NaCl, pH7.5, 0.5 mM TCEP, 10 mM imidazole, 1 mM PMSF, 10 μ g/mL DNase, 0.125 mg/mL lysozyme) and lysed for 15–20 min using an ultra-sonicator (pulse on for 7 s and pulse off for 20 s, 27 % amplitude). The lysate was then subjected to centrifugation at 14400g for 40 min, and the supernatant was collected, filtered, and loaded to HisTrap column (GE Healthcare) equilibrated with Buffer A (25 mM Tris, 300 mM NaCl, pH7.5, 0.5 mM TCEP, 10 mM imidazole). The protein was eluted with buffer B (25 mM Tris, 300 mM NaCl, pH7.5, 0.5 mM TCEP, 500 mM imidazole) and further purified using a HiPrep™ 26/10 Desalting column (GE Healthcare) equilibrated with desalting buffer (50 mM Tris, 150 mM NaCl, pH7.5, 0.5 mM TCEP). The protein was concentrated to ~15 mg/mL and stored at –80 °C.

2.2. Compound library description

A total of 172 drugs from the *in-house* library of the Drug Bank of Dr Panjwani Center for Molecular Medicine and Drug Research (ICCBS) were grouped into 60 mixtures with 2–5 compounds in each mixture (Table-S2). The compounds were prepared initially at 100 mM stock in DMSO- d_6 and then diluted to 1 mM in NMR buffer (Tris- d_{11} 50 mM; NaCl 150 mM; TCEP 0.5 mM; pH 7.5). The use of mixtures significantly reduces the NMR experimental time but necessitates the individual validation of potential binders in active mixtures.

2.3. Saturation transfer difference (STD) NMR experiment

NMR experiments were performed on Avance NEO 600 MHz NMR spectrometer (Bruker, Switzerland) at 298 K. The magnet was equipped with a 5 mm inverse triple-resonance cryoprobe and automated sample changer (SampleCase™, Bruker, Switzerland). The folding of protein was evaluated by a 1H NMR experiment (Supplementary Fig. S1). In the ligand-based STD-NMR experiment, the on- and off-resonance irradiation frequencies were set at –134 Hz (–0.22 ppm) and 18,000 Hz (30 ppm), respectively. The on-resonance irradiation frequency targets the methyl resonances of the catalytic domain of USP7 (USP7-CD). NMR samples (0.55 mL) containing ligand to protein with a molar ratio 100:1 were prepared in tris- d_{11} buffer (prepared in 10 % D_2O and 90 % H_2O). Pulse sequence *stdiffesgp.3* from the Bruker library was used to record the STD-NMR experiment, where the water signal was suppressed using an excitation sculpting pulse program [12]. Relaxation delay and saturation time were 3.1 and 3 s, respectively. The number of dummy scans and scans were 16 and 1024, respectively; the spin lock duration was set to 30 ms with 4960 Hz power. For the selective irradiation, a train of 40 Gaussian pulses with a field strength of 86 Hz was used; each pulse had a length of 50 ms and was separated by a 0.1 s delay. The STD amplification factor of each proton of ligand showing the interaction with protein was calculated by using the following formula:

$$\text{STD Amplification Factor} = \left(\frac{I_{\text{std}}}{I_0} \right) \times \text{Ligand Excess},$$

where I_0 and I_{std} are intensities of the signal in the off-resonance and difference NMR spectra, respectively.

The affinity of the compounds towards USP7-CD was determined by titrating the protein with increasing concentrations of the compounds [12]. The dissociation constant (K_d) values were measured by fitting the signal intensities in STD titration spectra using GOSA software and the following equation:

$$\text{STD Amplification Factor} = A_{\text{max}} \times \frac{[L]}{[L] + K_d}$$

where $[L]$ is the ligand concentration, and A_{max} is the maximum amplification factor [12].

2.4. Thermal shift assay (TSA)

The thermal shift assay was performed on a real-time PCR machine (Bio-Rad Laboratories, USA), following the method described by Niesen et al., 2007 [13]. All samples were prepared in the buffer containing 50 mM Tris, 150 mM NaCl, 0.5 mM TCEP, and pH 7.5. Samples containing USP7 (10 μ M), ligands (1 mM), and Sypro®Orange dye (1:1000) were heated in the PCR tubes at a rate of 0.3 °C/min from 20 to 99.9 °C. The fluorescence intensity of the dye as a function of temperature was recorded using the HEX (Ex/Em: 538/555 nm) channel. Duplicates were performed for each protein/ligand ratio, and each experiment was repeated at least thrice.

2.5. Molecular docking studies

To get structural insights into ligand-protein complex, the co-crystal structure of USP7-CD with non-covalent inhibitor FT671 (PDB ID: 5NGE) was used for the *in silico* studies [14,15] using the Glide 6.9 module of the Schrödinger suite of programs, version 2020-2 [16–25]. The protein preparation wizard tool and OPLS3 force field were employed for protein preparation, minimization, and optimization. The ligand molecules were prepared using Schrödinger's LIGPREP module, which generates the correct protonation and possible ionization states. A receptor grid was generated around the centroid of the co-crystallized ligand (FT671) with a grid box of 10 \times 10 \times 10 Å. The Glide XP module was used to dock the ligands, and results were analyzed for the best-docked poses [18,19]. Molecular mechanics with generalized Born and surface area solvation (MMGBSA) was used to further validate the docked poses by evaluating the binding free energies of the ligand-receptor complex. For this, the Prime module from the Schrödinger suite was used with default settings.

2.6. Molecular dynamics simulations

Docked protein-ligand complexes were subjected to MD simulations using Desmond of the Schrödinger software suite to assess the time-dependent changes in structural and dynamical properties of the complexes over a simulation time of 100 ns. The simulation system was set up in periodic orthorhombic boxes and the SPC water model was employed to solvate the complexes. The system was neutralized by Na⁺/Cl⁻ ions, and 0.15 M NaCl was added to mimic physiological conditions. The simulations were performed in an NPT ensemble at a constant temperature of 310K and pressure of 1 Bar.

2.7. In vitro anti-proliferation activity against colorectal cancer (HCT116) cells

Compounds that showed binding with the USP7-CD, and had a negative effect on the thermal stability of the protein were further evaluated for their anti-cancer (cytotoxic) effect on HCT-116 cells via tetrazolium-based MTT assay, as described below [26]. Expression of USP7 is reported to be high in colorectal cancer; therefore, these cells were used in the cellular studies [27]. In this assay, MTT reduction by mitochondrial enzyme was measured spectrophotometrically. MTT reduction can only occur in metabolically active cells, and these studies, therefore, give an idea about the effect of test compounds on cell viability.

Briefly, human fibroblast and colorectal cancer cells were cultured in Dulbecco's Modified Eagle Medium (DMEM), supplemented with 5% of Fetal Bovine Serum (FBS), 100 IU/mL of penicillin and 100 μ g/mL of streptomycin, and kept at 37 °C in 5% CO₂ incubator. Cell culture at the concentration of 5 \times 10⁴ cells/mL was prepared and introduced into 96-well plates. After overnight incubation, the medium was removed, and a fresh medium with different concentrations of compounds was added. After 48 h, MTT (0.5 mg/mL) was added to each well and incubated further for 4 h. Subsequently, DMSO was added to each well. The extent of MTT reduction to formazan was measured at 540 nm using a microplate reader (SpectraMax Plus, Molecular Devices, CA, USA). Each experiment was run in triplicate.

2.8. Quantitative Gene Expression Analysis

Compounds with anti-cancer activity were then evaluated for their effect on the expression of tumor suppressor (p53) and proto-oncogenes (MDM2, c-Myc) in HCT-116 cells via RT-PCR. Briefly, HCT-116 cells (2 \times 10⁵ cells) were seeded in 6-well plates in standard cell culture conditions. On reaching confluence, compounds were added at their IC₅₀ concentration, and cells were incubated further

for 48 h. Following incubation, cells were harvested, and RNA was isolated by the TRIzol method, as described previously [28]. The RNA concentration was determined using NanoDrop 2000 (Thermo Scientific, USA). The cDNA for the isolated RNA was synthesized using the Revert Aid First-strand cDNA synthesis kit, following the manufacturer's protocol (Thermo Scientific, USA). Sequences of the primers for the studied genes are provided in supplementary Table-S3. Genes of interest, *i.e.*, MDM2, USP7, p53, and c-Myc, were amplified using qPCR with SYBER Green PCR master mix (Thermo Scientific, USA) in CFX-96 Real-time PCR (Bio-Rad Laboratories, USA). GAPDH was used as a housekeeping gene for normalization. The Cq values were used to quantify gene expression in fold change. Fold change in gene expression was calculated using the following formula:

$$\text{mRNA Levels (Fold Change)} = 2^{-\Delta\Delta\text{CT}}$$

where $\Delta\Delta\text{CT} = (\text{gene of interest-gene of treated group}) - (\text{GAPDH of treated group-GAPDH untreated group})$

2.9. Data analysis

The data acquired from NMR experiments was analyzed through Topspin-Software 4.3.1 (Bruker, Biospin GmbH, Germany), while the K_d values were measured by fitting the signal intensities in STD titration spectra using GOSA software. For thermal shift assay, the fluorescence intensity of the dye as a function of temperature was recorded using the HEX (Ex/Em: 538/555 nm) channel, and the data was analyzed via CFX 96 Manager™ software (Bio-Rad Laboratories, USA). The EZ-Fit enzyme kinetics program (Perrella Scientific Inc., Amherst, USA) was employed to calculate the IC50 values for the antiproliferative activity. Experiments were run in triplicate, and the IC50 values were reported as mean \pm standard deviation (SD). For quantitative Gene Expression Analysis, data was analyzed using SPSS, statistics version 21.0 (SPSS, Inc, USA). The Student's *t*-test and one-way ANOVA with post hoc Dunnett's test were used to determine the statistical differences (***P* < 0.01, **P* < 0.05).

3. Results and discussion

A total of 172 US-FDA-approved drugs were evaluated against the catalytic domain of the USP7 enzyme using biophysical techniques, followed by molecular docking and simulation studies to get structural insights about protein-ligand complexes. In the next stage, the newly identified active compounds were studied for their ability to inhibit the proliferation of colorectal cancerous cells (HCT116). This was followed by analyzing their effects on the expression level of proto-oncogenes, and tumor-suppressor genes in HCT116 cells.

3.1. Analysis of compounds binding to the USP7-CD by STD-NMR

Ligand-based NMR screening via saturation transfer difference NMR (STD-NMR) experiments plays an important role in the rational drug discovery process. Based on the NOE principle, it is an excellent technique for the identification of ligands of moderate to weak affinity (K_d ranges from mM to μM) towards a macromolecule or receptor [26].

The STD-NMR experiment involves selective saturation of the macromolecule that spreads over the surface of the macromolecule via spin diffusion. This saturation can also be transferred to the ligand (through intermolecular NOE) if it is bound to or in a close vicinity of the macromolecule. The ligand then dissociates from the macromolecule and transfers the saturation into the solution, where it can be detected. Information embedded in the STD-NMR experiment can be used to map the orientation of the ligand on the protein surface, *i.e.*, group epitope mapping (GEM). However, detailed structural insights about the ligand-protein complex are limited, as the protein is not under direct observation.

In GEM analysis, proton(s) with the largest STD integral value is set to an arbitrary value of 100%, and STD integrals of all other protons are normalized against it. This provides the relative degrees of saturation received from protein by individual protons. The degree of saturation of the individual protons of a ligand molecule reflects their proximity to the biomolecule surface. Moieties that are in close proximity to protein will receive more saturation, in comparison to distant ones ($>5 \text{ \AA}$) [11,25,26].

During the current study, 30 compounds from the mixtures 1, 6, 12, 13, 15, 17, 19, 20, 31, 32, 36, 39, 55, 56, and 59 showed interactions with the USP 7-CD in STD-NMR experiments (Table S2). The compounds in these mixtures were then evaluated individually for the STD- NMR experiments, and 11 drugs (Table 1) exhibited their ability to bind with the USP7-CD.

Furthermore, the affinity of the compounds in terms of the K_d towards USP7 was calculated by using STD-NMR titration experiments. The K_d values rely on the exchange between free and protein-bound states of the ligand. High-affinity ligands cannot be identified via STD-NMR as tight ligand binding results in low dissociation (k_{off}) rates, due to which the ligand spends more time in the protein binding pocket. Efficient spin diffusion causes the ligand to relax before it can accumulate the saturation in the solution, impeding the transfer of saturation from the bound ligand into the solution, and therefore, no STD NMR effect can be observed. On the contrary, when a ligand binds very weakly, the likelihood of the ligand staying in the receptor site is very low, resulting in either no or very weak STD signals. The ligand must be in fast exchange between the free and bound states on the NMR timescale for optimal exchange. Since relaxation is less efficient in small molecules, it may lead to efficient build-up of the ligand molecules in solution [29–31].

Compounds 1 (bromofenac sodium) and 2 (diclofenac sodium) are anti-inflammatory and analgesic drugs [32,33]. In compound 1, the H2'/H6' signal displayed the highest STD integral value, and was set to receive 100% saturation from the protein (supplementary file 2). The relative saturation of other protons was then calculated with reference to the integral value of H2'/H6'. The H5'/H3'

received 88% saturation, followed by H4/H6 and H5, which received 73 and 78% relative saturation, respectively. The H-2'' achieved only 28% relative saturation. The GEM analysis suggested that the H2'/H6' are in close proximity to the protein, while methylene protons (H-2'') are located a little far (but at a distance <5 Å) from the protein (Fig. 1 a, b). Compound 1 interacted with protein with a moderate affinity with K_d value of 0.78 ± 0.53 mM.

For compound 2, the signal for H3'''/H5''' with the highest integral value was set to receive 100% saturation from the protein (supplementary file 2). The H3''' signal received 87% relative saturation, followed by H4'''/H4'''/H5''', and H6''' signals, which showed 78, 73, 72, and 54% relative saturations, respectively. Epitope mapping clearly indicated that the H3'''/H5''' are in direct contact with the protein (Fig. 2a, b). Methylene protons (H-2'') did not show any STD effects. Compound 2 interacted with a moderate affinity, as indicated by a K_d value of 0.76 ± 0.56 mM.

Compound 3 (ketoprofen) is a nonsteroidal anti-inflammatory drug (NSAID) [34]. The H3/H5 signal with the largest integral value was set to achieve 100% saturation (supplementary file 2). This was followed by H4, and H2/H6 signals with 98 and 85% of relative saturation, respectively. The H2'/H4', and H5'/H6' signals showed 75 and 77% of relative saturation, respectively. The lowest relative saturation (17%) was displayed by the H2'', indicating that it may be located far from the protein binding site. GEM analysis, indicated that benzoyl ring protons of compound 3 are directly involved in the binding to protein (Supplementary Fig. S2). From STD titration experiments, it was found that compound 3 has relatively high affinity (K_d : 0.62 ± 0.56 mM) for the protein, as compared to compounds 1 and 2 that showed K_d values of 0.78 and 0.76 mM, respectively.

Compound 4 (labetalol hydrochloride) is a drug used for the treatment of hypertension [35]. The H6'''/H2'''/H4 signal with the largest integral value was arbitrarily assigned to receive 100% saturation from the protein (supplementary file 2). The H3 signal received 93% relative saturation, while H3'''/H4'''/H5''' signals received 67% relative saturation. This was followed by H6 and H1'' signals that exhibited 48 and 39% relative saturation, respectively. GEM analysis indicates that the H6'''/H2'''/H4 and H3 have close contact with the protein (Supplementary Fig. S3). Compound 4 displayed a weak affinity towards the protein with a K_d value of 0.91 ± 0.70 mM.

Compound 5 (orphenadrine) is a drug for gastrointestinal ulcers and constipation [36]. The STD experiment on compound 5 showed the largest integral value for the H3''' signal, and thus, it was set to be 100% saturated from the protein (supplementary file 2). This was followed by H4', H4'', and H5'', which received 94–97 % relative saturation. Further, the relative saturation of the signals for H5'/H3' and H2'/H6' was found to be 80 and 79%, respectively. The H6'', H2'', and H7' signals were saturated up to 68.53, 68.35, and 53 %, respectively. The methyl and methylene groups showed low relative saturation (30–39%), indicating their distant location from the protein (Supplementary Fig. S4). Compound 5 had a low affinity as the K_d was determined to be 1.1 ± 0.80 mM.

Compound 6 (oxybutynin) treats bladder malfunctions, and is also used for autophagy-related diseases [37]. The H5/H3 signals have the highest integral value and are therefore proposed to have 100% saturation from the protein (supplementary file 2). The relative saturation of other signals (H6/H4/H2/H2''/H2''') was in the range of 91–96%. The H1''/H1'''/H1'''' signals showed 64–68% relative saturation. The H4'' signal showed 17% relative saturation, which means it is a bit further away from the protein (Supplementary Fig. S5). The GEM analysis indicated that H5/H4/H3 protons are directly involved in binding to the protein. This indicated that they are positioned at a distance within the range of 5 Å. STD titration studies indicated that compound 6 has a relatively high

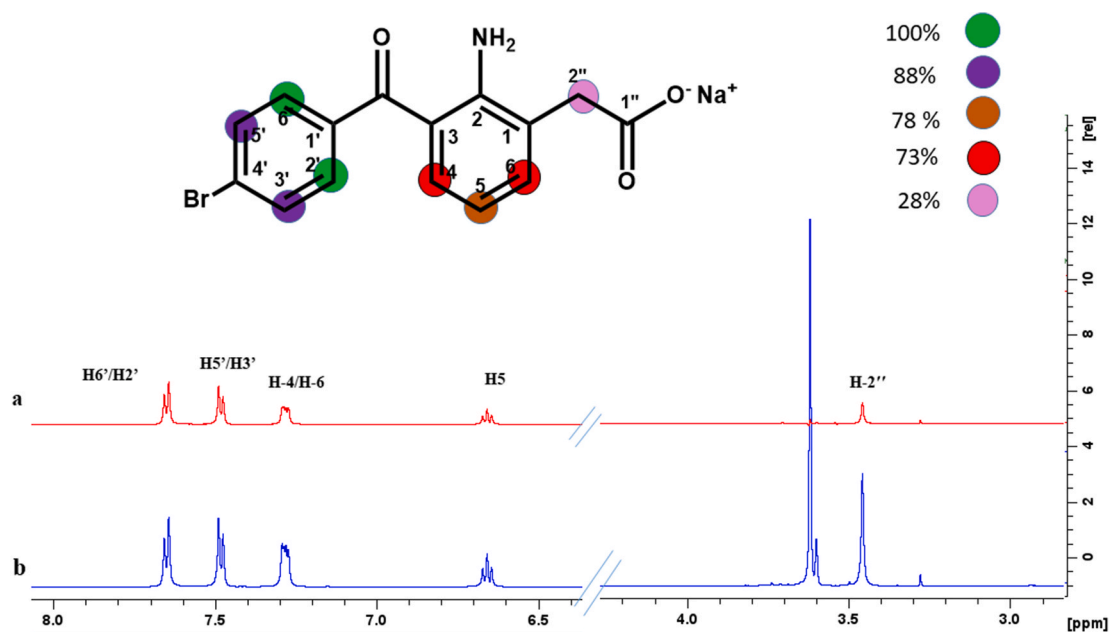


Fig. 1. STD-NMR Analysis of Compound 1. a) STD difference spectrum in the presence of USP protein (red); b) ^1H NMR (off-resonance) spectrum (blue) of compound 1. Relative saturation (%) of signals normalized to that of the H2'/H6' signal is indicated with a color code.

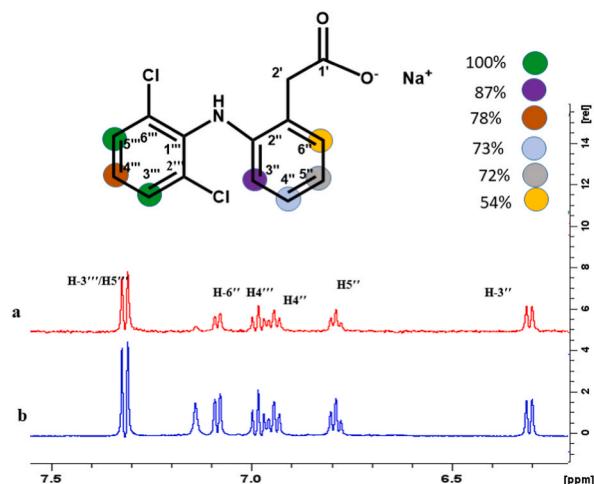


Fig. 2. STD-NMR Analysis of compound 2. **a)** STD difference spectrum in the presence of USP protein (red); **b)** ^1H NMR (off-resonance) spectrum (blue) of compound 2. Relative saturation (%) of protons normalized to that of the $\text{H}3''/\text{H}5''$ is indicated with a color code.

affinity towards protein, showing a K_d value of 0.66 ± 0.46 mM, comparable to compound 3 (K_d : 0.62 ± 0.56 mM).

Compound 7 (ketotifen) is an antihistamine drug [38]. Its $\text{H}2'$ signal was set to receive 100% saturation, as it showed the highest integral value (supplementary file 2). This was followed by the signals of $\text{H}3''$, $\text{H}4''/\text{H}1''/\text{H}2''$, and $\text{H}3'$, which received 66, 64, and 51% of relative saturation, respectively. The $\text{H}2/\text{H}3/\text{H}5/\text{H}6$ protons did not appear in the difference spectrum, indicating their far proximity from the protein. The GEM analysis, therefore, indicated that $\text{H}2'$ is involved in the binding with USP7 protein (Supplementary Fig. S6). STD titration studies showed that compound 7, with K_d 1.1 ± 0.88 mM, has a weak affinity towards protein.

Compound 8 (ticlopidine hydrochloride) has anti-platelet activity, and is used for treating thrombotic strokes [39]. Its $\text{H}2$ signal was set to be 100% saturated from protein (supplementary file 2). With reference to $\text{H}2$ signal saturation, the $\text{H}3$ and $\text{H}5'$ signals received 77 and 64% saturation, respectively. The $\text{H}4'$ and $\text{H}3'/\text{H}6'$ signals showed 55–59% relative saturation, respectively. The $\text{H}4$ and $\text{H}7$ did not appear in the STD difference spectrum as they might be located far from the protein binding site. The GEM analysis conferred that $\text{H}2$ was in close contact with the protein (Supplementary Fig. S7). Compound 8 was found to possess the lowest affinity (K_d : 1.49 ± 1.41 mM) towards the protein among the evaluated compounds (Table-1).

Compound 9 (lamotrigine) is a US-FDA approved molecule for the treatment of epilepsy and bipolar disorders [40]. The $\text{H}4'$ signal with the highest integral value was set to achieve 100% saturation from the macromolecule (supplementary file 2). This was followed by $\text{H}5$ and $\text{H}6$ signals that showed 65 and 59% relative saturation, respectively (Supplementary Fig. S8). The K_d value of 1.0 ± 0.56 mM indicated that compound 9 has low affinity towards USP7.

Compound 10 (pantoprazole sodium) is used to treat stomach and esophagus problems [41]. Its $\text{H}4$ signal, with the highest integral value in the STD spectrum (100%), was used as a reference (supplementary file 2). The $\text{H}10'$, $\text{H}5$, $\text{H}7'$, and $\text{H}6$ signals showed 92, 73, 67, and 60% relative saturation, respectively. The $\text{H}6'$ and $\text{H}1$ signals have lower relative STD values (31–34%), indicating their location at a more distant position to the protein (Supplementary Fig. S9). Compound 10 is a moderate affinity binder (K_d : 0.87 ± 0.28 mM) for USP7.

Compound 11 (escitalopram) is used for the management of anxiety and depression [42]. The $\text{H}4/\text{H}6$ signal with the highest integral value was set to 100% saturation, followed by the $\text{H}3''/\text{H}5''$ signal, which showed 90% relative saturation (supplementary file 2). The $\text{H}2''/\text{H}6''/\text{H}3$ signal achieved 55% relative saturation, while the $\text{H}8$ signal has 24% relative saturation. The epitope mapping, therefore, indicated that $\text{H}4/\text{H}6$ and $\text{H}3''/\text{H}5''$ were in direct contact with protein, while $\text{H}8$ was located at a distant position as it showed relatively less saturation (24 %) (Supplementary Fig. S10). Compound 11 has a low affinity for USP7 (K_d : 1.22 ± 1.12 mM).

The affinity or the strength with which a ligand binds to a protein is not directly correlated to biological activity. Ligand-protein complexes with low-affinity interactions may have important and critical biological consequences, while high-affinity interactions between protein and ligand may have lower specificity and biological importance [43]. Therefore, the results discussed need to be validated by other methods.

3.2. Analysis of drug binding to USP7-CD by thermal shift assay

Thermal shift assay (TSA) is a general tool for the hit identification against the targets for which physiological substrates are either unknown or difficult to synthesize [44]. For the USP7 enzyme, the substrates are ubiquitin-rhodamine or ubiquitin-AMC, which are expensive or challenging to synthesize; therefore, a thermal shift assay was used to assess the ability of the test compounds to destabilize the USP-CD. In this experiment, thermal unfolding of biomolecules (in terms of melting temperature; T_m) was studied in the presence of a fluorescent dye. The T_m is the temperature at which folded and unfolded protein states are equally populated. Changes in the T_m , upon ligand (test compounds) addition, reflect changes in a biomolecule's thermal stability. Changes in the free energy of the

protein due to ligand binding may result in an increase (or decrease) in the T_m , and reflect their stabilization (or destabilization) effect on the protein.

The T_m of USP7-CD in the absence of any ligand was found to be 45 °C, which aligns with the T_m value reported previously [45]. The 11 compounds that showed binding in STD-NMR were able to reduce the USP7-CD melting temperature, indicating that they were negative modulators of USP (Fig. 3, Supplementary Figs. S11–S14, Table-1). The standard compound (HBX41108) reduced the T_m of USP7-CD by more than 6 °C. The HBX 41,108 is a cyano-indenopyrazine derivative that causes USP7 inhibition with $IC_{50} = 0.424 \mu\text{M}$. It is an uncompetitive inhibitor. Compounds 1, 8, 10, and 11 showed the strongest destabilizing effect as they reduced the T_m of USP7-CD by more than 9 °C. Compounds 9 and 7 decreased the T_m of USP7-CD similarly to that of standard (HBX41108), while compounds 2–6 induced a relatively small decrease in T_m (up to 4 °C) of USP7-CD (Table-1).

3.3. Molecular docking studies

The fold of the catalytic domain of USP7 can be described as a right hand, with three sub-domains as fingers, palm, and thumb, formed by a combination of α -helices, tight turns, and β -sheets, respectively. These sub-domains create a prominent binding pocket for the ubiquitin between the fingers-palm-thumb scaffold (Supplementary Fig. S15). A deep catalytic cleft is formed between the anti-parallel β sheet of the palm and the α -helices of the thumb. The highly conserved cysteine box and histidine box are located on the opposing sides of the cleft. The catalytic triad contains Cys223, His464, and Asp481. During the catalysis, Cys223 undergoes deprotonation, which is assisted by an adjacent His464, which, in turn, is stabilized by a nearby Asp481 [8,9].

After the protein preparation, the co-crystallized ligand (FT671) was re-docked to validate the structure of the minimized protein, and subsequent docking results. The root mean square deviation (RMSD) of 0.472 Å was observed between the co-crystallized and re-docked complex. Most of the interactions were retained in the docked pose, such as hydrogen bonds with Gln297, Asp295, Phe409, Val296, and Try465, while aromatic hydrogen bonds with Tyr224, Asp295, Gln297, Phe409, and π - π stacking interactions with Phe409, and His456 (Supplementary Figs. S16 and S17) [8,9,11]. The standard compound also interacted with the catalytic cleft via hydrogen bonding to the Gln297 and Arg408 residues and aromatic hydrogen bonding to Phe409 (Supplementary Fig. S18).

All the compounds showed binding in the palm-thumb catalytic cleft of USP7, where they make extensive contacts with various residues of the enzyme as shown in Fig. 4 (a, b), Fig. 5 (a, b), and Supplementary Figs. S19–27. The docking scores were in the range of -5.94 to -7.85 . The binding energies were also large and negative (-39 to -73.79 kcal/mol), indicating better binding of these ligands with USP7. The interactions of these compounds is provided in supplementary Table-S4. Compounds interacted with highly conserved residues, such as Asp295, Gln297, His461, Phe409, and Tyr465 via non-covalent interactions. The two-dimensional Ligplot representation of all the complexes' molecular docking interactions is given in Supplementary Fig. S28. The ubiquitin (substrate) actually binds in the catalytic cleft of USP7, and is catalyzed by the enzyme. The binding of active compounds in this site may block the entry of ubiquitin, thereby inhibiting the activity of USP7 (see Fig. 5).

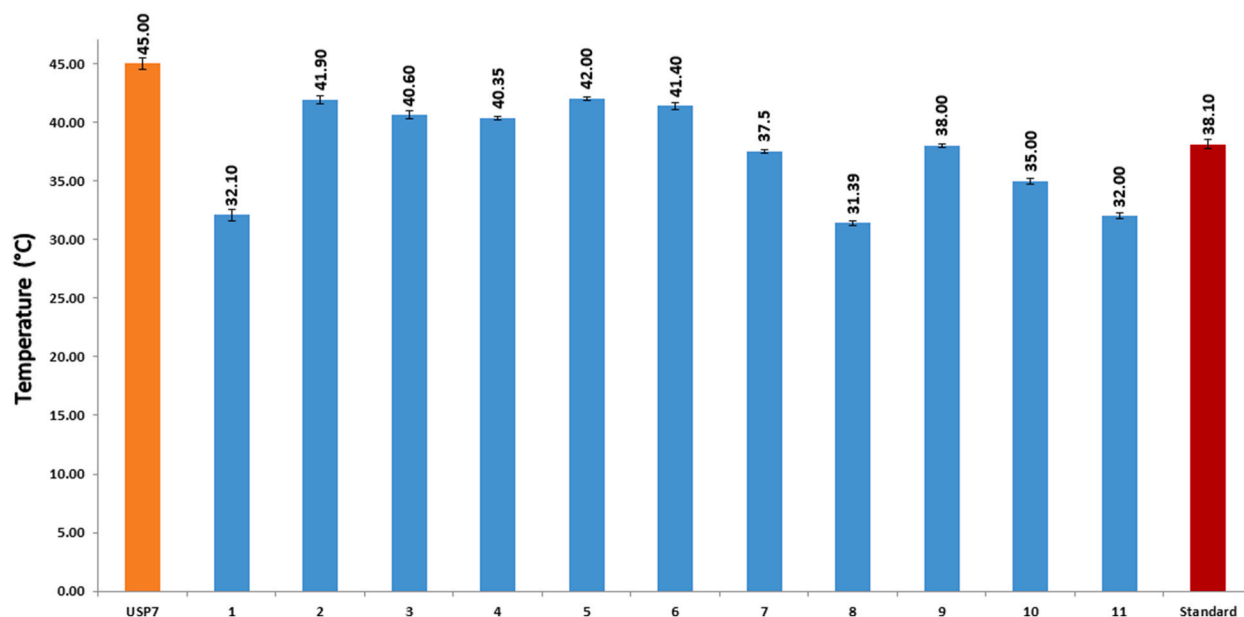


Fig. 3. Changes in T_m values of the catalytic domain of USP7 upon addition of the drugs. The T_m value for USP7-CD alone is in orange color, the standard is in maroon color, while blue bars correspond to the drug molecules whose addition showed the change in protein's T_m .

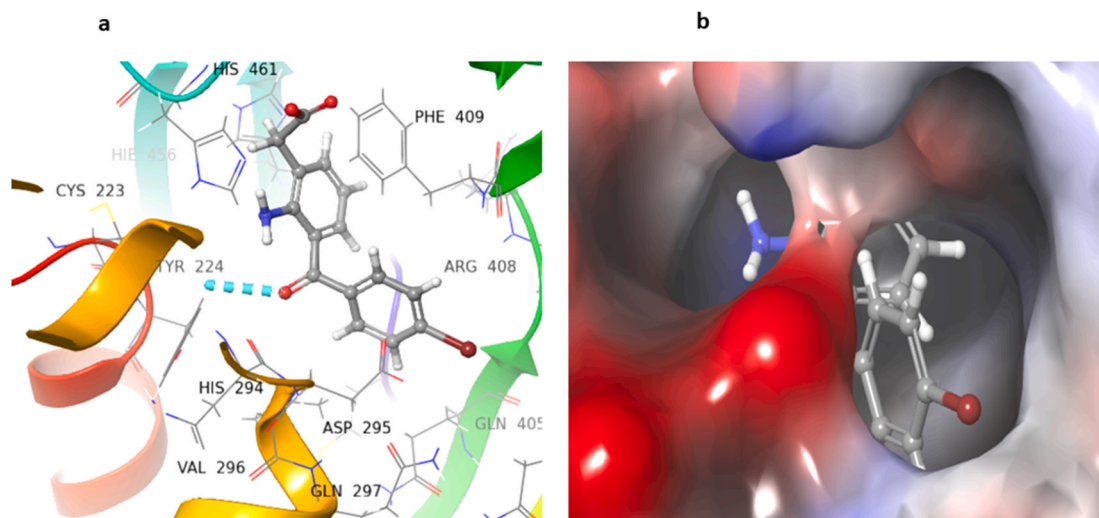


Fig. 4. Docked pose of compound 1: a) Compound 1 (Grey sticks with colored non-carbon heavy atoms) docking with USP7-CD (Ribbon representation of the backbone with important side chains shown with grey lines) b) 3D Molecular surface representation of docked pose of compound 1 in the USP7-CD.

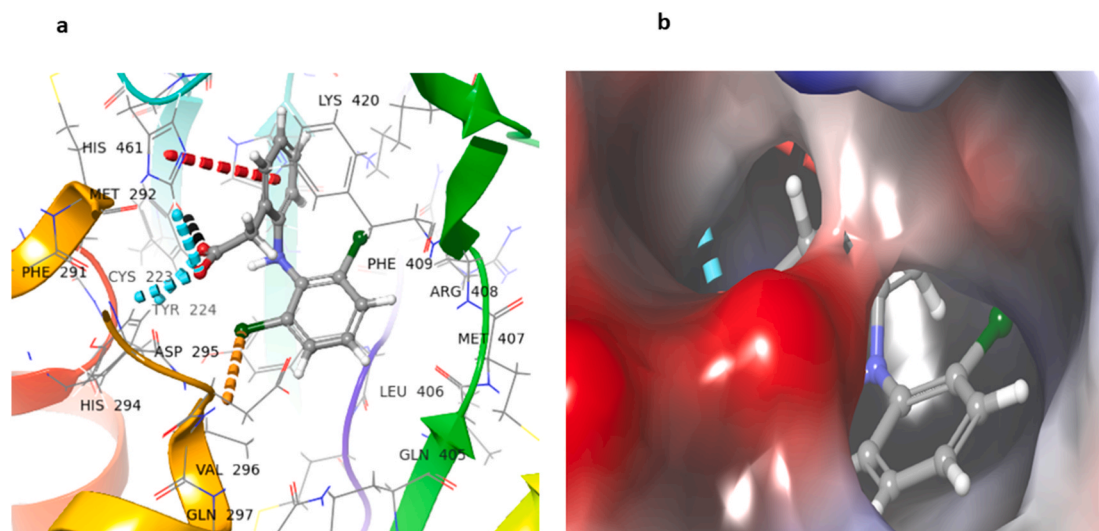


Fig. 5. Docked pose of compound 2: a) Compound 2 (Grey sticks with colored non-carbon heavy atoms) docking with USP7-CD (Ribbon representation of the backbone with important side chains shown with grey lines) b) 3D Molecular surface representation of docked pose of compound 2 in the USP7-CD.

3.4. Coherence between STD-NMR and molecular docking studies

The results of docking studies were in agreement with the epitope mapping, analyzed in STD-NMR studies with few differences. It is worth mentioning that in the STD-NMR experiment, exchangeable protons (such as OH and NH groups) are not detected, while in docking studies, one can analyze all the functional groups present in a ligand.

The carbonyl group of compound 1 showed aromatic hydrogen bonding with Tyr224, and its phenyl rings made hydrophobic interactions with the USP-CD residues. Similarly, the aromatic protons of these rings showed significant STD effects. The unsubstituted phenyl rings in compounds 2, 3, and 4 showed π - π stacking interactions, and the protons of these rings also showed stronger STD effects. In compound 5 only a salt bridge was observed with Asp295, while both the aromatic rings can form hydrophobic contacts, while in STD-NMR, these rings showed major STD effects. In compound 6, the aromatic protons of the phenyl and cyclohexane rings showed aromatic hydrogen bonding, while in STD-NMR, the phenyl ring showed major STD effects. In compound 7, the unsubstituted phenyl ring showed aromatic hydrogen bonding, while this ring also showed STD effects. In compounds 8 and 9, the Cl-substituted phenyl ring showed π - π stacking interactions, while this ring also showed an effect in STD-NMR. The fluorine-substituted phenyl

rings in compounds **10** and **11** showed aromatic hydrogen bonds, and these rings also showed significant STD effects.

3.5. *In vitro* anti-cancer activity against colorectal cancer (HCT116) cells

The anti-cancer effects of compounds **1–11** on HCT116 were analyzed using an *in-vitro* MTT assay. Compounds **6**, **7**, **10**, and **11** inhibited the proliferation of cancer cells (Fig. 6 a, b, Supplementary Figs. S29 and S30) with IC₅₀ values in the range of 36.25 ± 1.03 to 227.6 ± 0.71 μM, in comparison to the standard drug, Tunicamycin (IC₅₀ = 0.24 ± 1.03 μM). Compounds **1–5**, **8**, and **9** were found to be inactive as they did not inhibit the proliferation of cancerous cells. Compounds **6**, **7**, **10**, and **11** were further studied for quantitative PCR analysis.

3.6. Quantitative PCR analysis

The effects of compounds **6**, **7**, **10**, and **11** were next studied on the mRNA expression of proto-oncogenes (USP7, MDM2, and c-Myc), and tumor-suppressor gene (p53). The MDM2 and p53 genes are among the most important oncogenes relevant to carcinogenesis. Increased mRNA expression of MDM2 may increase the production of MDM2 protein, which in turn reduces the cellular concentration of p53 by causing its ubiquitination, and subjecting it to proteasomal degradation [46–50]. The transcription factor c-MYC is a master regulator for cell metabolism and proliferation, and its mRNA level is quite low in healthy cells. However, in tumor cells, its expression is increased due to the unregulated oncogenic signals such as USP7, which subsequently increase the proliferation in cancer cells. High expression levels of proto-oncogenes, and low cellular concentrations of p53 are reported to activate the WNT signaling pathway, which facilitates cancer progression by promoting cell proliferation and inhibiting the apoptosis processes [51,52].

Untreated colorectal cancer cells showed high mRNA levels for USP7 and proto-oncogenes, while the level of the p53 gene was low. Compounds **6**, **7**, **10**, and **11** significantly decreased the mRNA expression ($P < 0.01$) of proto-oncogenes. In contrast, the mRNA expression of the tumor suppressor gene (p53) was significantly ($P < 0.05$) increased by compounds **6** and non-significantly by compounds **7**, and **11** (Fig. 7 a, Fig. 7b-d). Compound **10** did not cause an increase in the mRNA expression of p53 (Fig. 7c). Therefore, it can be proposed that compounds **6**, **7**, **10**, and **11** inhibit cancer cell proliferation by reducing the mRNA expression of proto-oncogenes, and possibly their expression at the protein level. High levels of proto-oncogenes and proteins can activate the WNT signaling pathway in cancer cells. These compounds are proposed to possess anti-cancer effects primarily by inhibiting the WNT pathway. They further contribute to restoring the p53 expression level in the cancer cells, which causes the cancer cells to undergo apoptosis. This conclusion is proposed based on previous findings of the involvement of USP7 inhibitors in downregulating the WNT signaling pathway by reducing the expression of various proto-oncogenes, and restoring the p53 pathway [49–54].

3.7. Molecular dynamics (MD) simulations

Classical MD simulation employs metrics such as RMSD for predicting stability and discerning conformational shifts in receptor complexes [55]. RMSD is a measure of the average distance between atoms of superimposed proteins. In the context of molecular dynamics, RMSD is often used to assess how much a particular structure (protein or ligand) has changed from a reference conformation over the course of the simulation. A 100 ns MD simulation for USP7 without any ligand was initially performed to assess the stability of the protein and create a reference for subsequent MD simulation studies. The protein remained stable throughout the stimulation

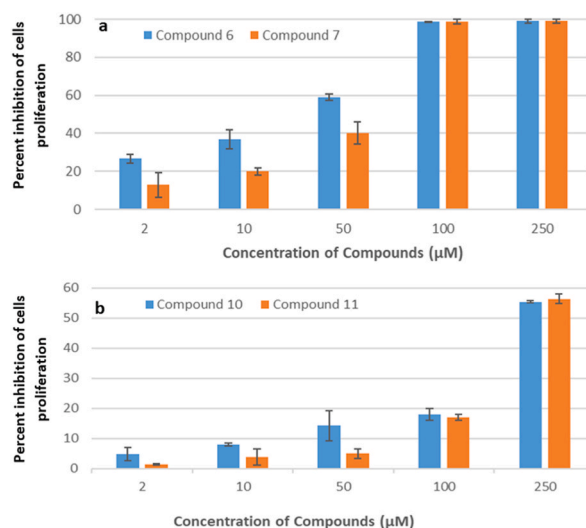


Fig. 6. Graphical representation of percent inhibition of proliferation of HCT-116 cell. a) Percent inhibition of proliferation of HCT-116 cells in the presence of compounds **6** and **7**. b) Percent inhibition of proliferation of HCT-116 cells in the presence of compounds **10** and **11**.

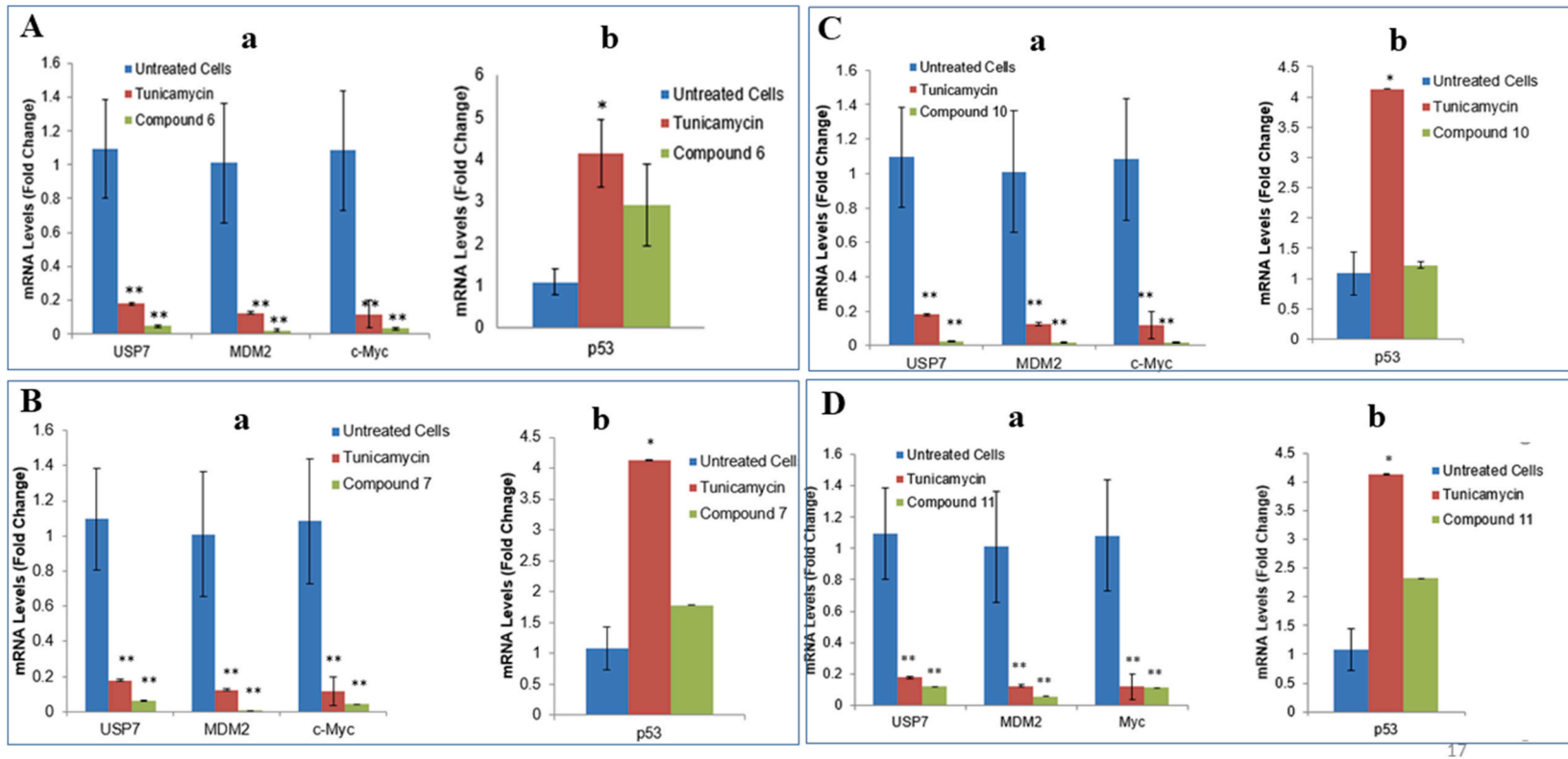


Fig. 7. (A) Effect of compound 6 on the gene expression of (a) proto-oncogenic USP7, MDM2, and c-Myc, (b) tumor-suppressor p53. The mRNA expression levels (fold change) in HCT116 cells: untreated cells (blue bars, negative control), treated with Tunicamycin (red, positive control) or compound 6 (green), * $p \leq 0.05$, and ** $p \leq 0.01$. (B) Effect of compound 7 on the gene expression of (a) proto-oncogenic USP7, MDM2, and c-Myc, (b) tumor-suppressor p53. The mRNA expression levels (fold change) in HCT116 cells: untreated cells (blue bars, negative control), treated with Tunicamycin (red, positive control) or compound 7 (green), * $p \leq 0.05$, and ** $p \leq 0.01$. (C) Effect of compound 10 on the gene expression of (a) proto-oncogenic USP7, MDM2, and c-Myc, (b) tumor-suppressor p53. The mRNA expression levels (fold change) in HCT116 cells: untreated cells (blue bars, negative control), treated with Tunicamycin (red, positive control) or compound 10 (green), * $p \leq 0.05$, and ** $p \leq 0.01$. (D) Effect of compound 11 on the gene expression of (a) proto-oncogenic USP7, MDM2, and c-Myc, (b) tumor-suppressor p53. The mRNA expression levels (fold change) in HCT116 cells: untreated cells (blue bars, negative control), treated with Tunicamycin (red, positive control) or compound 11 (green), * $p \leq 0.05$, and ** $p \leq 0.01$.

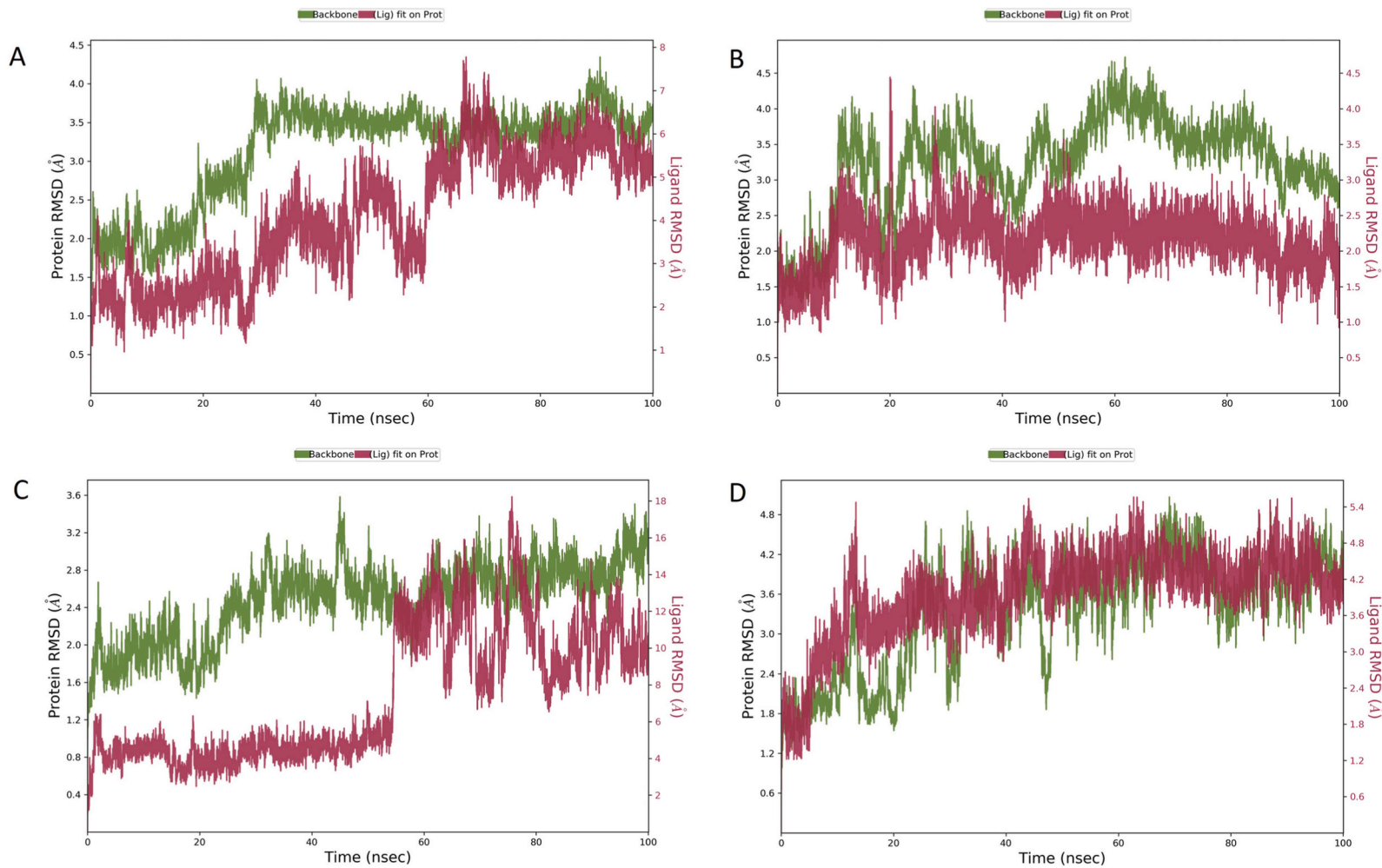


Fig. 8. Root mean square deviation (RMSD) plots for Molecular Dynamics (MD) simulations of USP7-CD with (A) compound 6, (B) compound 7, (C) compound 10, and (D) compound 11.

duration, with fluctuations observed between 1 and 3 Å, which are acceptable for small globular proteins. The RMSD and root mean square fluctuation (RMSF) plots for USP7 are given in [Supplementary Fig. S31](#).

Compounds **6**, **7**, **10**, and **11** were further subjected to MD simulation studies to improve the understanding of the protein-ligand complex. The graph ([Fig. 8](#)) shows the RMSD evolution of the protein (left Y-axis) and ligand fit on the protein (right Y-axis) for compounds **6**, **7**, **10**, and **11**. The green line represents the RMSD of the protein's backbone atoms from a reference conformation, measured in Angstroms (Å). It indicates how much the protein structure has fluctuated over time. A stable protein would have low and consistent RMSD values, while higher and more variable RMSD values could indicate more significant structural changes or flexibility. The burgundy line represents the RMSD of the ligand when it is fit onto the protein structure. This shows how the ligand's position and conformation change in relation to the protein over time. Similar to the protein RMSD, lower values indicate less movement from the initial conformation, suggesting a more stable interaction with the protein. The RMSF plots, characterizing local changes along the protein chain during MD simulation, for compounds **6**, **7**, **10**, and **11** are given in [Supplementary Fig. S32](#).

The RMSD of the protein in the presence of compound **6** ([Fig. 8A](#)) increased initially, which is typical as the system relaxed from its starting configuration. It fluctuated between roughly 2.5 and 3.5 Å throughout the simulation. However, the fluctuations were within a normal range for a globular protein. After 30 ns the protein RMSD showed a plateau, suggesting that the protein reached a state of dynamic equilibrium and simulation achieved convergence.

The ligand's RMSD showed greater variance, with values ranging approximately between 4 and 8 Å, indicating that the ligand experienced more substantial movements or conformational changes relative to the protein. The lack of plateau suggested that the ligand was not settled into a stable binding mode till 60 ns, after which the ligand achieved dynamic equilibrium, and the complex remained stable throughout the rest of the simulation time. This also supports the results from the thermal shift assay, where compound **6** was found to negatively modulate the protein. The histogram illustrating protein-ligand interactions during MD simulation revealed that Asp295 and Val296 were involved in forming hydrogen bonds, while Phe409 and Tyr514 made hydrophobic contact for more than 30% of the simulation time ([Supplementary Fig. S33A](#)).

In the RMSD plot for MD simulation of compound **7** ([Fig. 8B](#)), it can be seen that both the protein and the ligand exhibited fluctuations over the 100 ns simulation time. The protein's RMSD values were generally higher than the ligand's, suggesting that the protein's structure was more flexible or experienced more conformational changes than the ligand during this simulation period. However, the fluctuations were within a normal range for a globular protein. The ligand reached an equilibrium state after 50 ns and remained in the binding pocket of the protein throughout the stimulation duration. The overall trend did not seem to reach a plateau, which could imply that the protein and ligand were inherently dynamic, but the complex was stable throughout the simulation. This supported the results from the thermal shift assay, where we demonstrated that the binding of compound **7** with the protein reduced its T_m , thereby negatively modulating the USP7-CD. Regarding protein-ligand interactions, Gln405 and Tyr465 residues of USP7 established hydrogen bonds with compound **7**, while Tyr224, Val296, Phe409, His456, His461, and Tyr514 made hydrophobic contacts during more than 30% of the simulation time ([Supplementary Fig. S33B](#)). The RMSD plot for MD simulation of compound **10** ([Fig. 8C](#)) showed that the protein's backbone had a moderate level of stability, with RMSD values in the range of 1.2 Å and 4 Å, suggesting that while the protein's overall fold was maintained, there were fluctuations indicative of its dynamic nature. However, these fluctuations were within a normal range for a globular protein.

The ligand showed significantly higher RMSD values (approx. from 4 Å to over 16 Å), indicating that it underwent large movements or changes in conformation relative to the protein during the simulation. This could be due to the ligand moving in and out of the binding pocket or not being tightly bound to the protein. The ligand remained in the binding pocket for the initial 50 ns, after which it started fluctuating. Asp295, Val296, Gln297, Phe409, and Tyr411 residues of USP7 were involved in forming significant interactions with compound **10** ([Supplementary Fig. S33C](#)). In the thermal shift assay, compound **10** showed significant destabilizing activity by reducing the T_m of USP7-CD by more than 9 °C, but MD showed that compound **10** did not bind in this binding pocket so that it may bound to some other site of the protein present near the catalytic cleft.

During the MD simulation of the USP7-CD-compound **11** complex ([Fig. 8D](#)), the RMSD values for the protein and ligand increased initially, which is typical as the system relaxed from its starting configuration. The protein backbone RMSD fluctuated between approximately 1.2 Å and 3.6 Å, while for the ligand between approximately 2.4 Å and 4.8 Å. These values suggest that the protein experienced moderate conformational change throughout the simulation. The complex reached a plateau after 30 ns, suggesting that the complex reached a state of dynamic equilibrium and simulation achieved convergence. A stable complex was formed between uSP7-CDE and compound **11** that remained so throughout the simulation duration, corroborating our thermal shift assay results where compound **11**, on binding with USP7-CD, reduced its T_m , demonstrating negative modulation of the protein. Regarding protein-ligand interactions, Asp294 and Lys420 made hydrogen bonds with the ligand, while Val296, Phe409, and Tyr514 were involved in making hydrophobic contacts with compound **11** ([Supplementary Fig. S33D](#)). These results reveal that Asp295, Phe409, and Tyr514 are some of the key residues that interacted with the ligand during MD simulation studies.

4. Conclusion

Drug repositioning strategy is an efficient approach to identify new therapeutic indications of old drugs. It can expedite the drug discovery process as toxicological studies, pharmacokinetics/pharmacodynamics of the drugs, and their mechanisms of action are already documented. In this regard, 172 US-FDA-approved drugs were evaluated for their ability to destabilize the USP7 protein, a validated anti-cancer drug target. Compounds **1–11** showed binding with the catalytic domain of USP7 protein and negative modulation of its thermal stability. The protein-ligand interactions at the atomic level studied *via* molecular docking proposed that these compounds bind to the putative substrate binding pocket of USP7 and may block the entry of substrate, thereby inhibiting the enzyme.

Compounds **6**, **7**, **10**, and **11** also downregulated the expression of proto-oncogenes and upregulated the expression of tumor-suppressor genes. Thus, these compounds deserve to be investigated further at *in vitro* and *in vivo* levels for anti-cancer drug development.

Data availability statement

Data included in article/supp. material/referenced in article.

CRediT authorship contribution statement

Seema Zadi: Methodology, Formal analysis. **Sumaira Javaid:** Writing – original draft, Validation, Supervision, Resources, Project administration, Formal analysis, Data curation, Conceptualization. **Atia-tul-Wahab:** Writing – review & editing, Methodology. **Humaira Zafar:** Writing – review & editing, Methodology. **Muhammad Awais:** Methodology, Formal analysis, Data curation. **Innokentiy Maslennikov:** Writing – review & editing. **M. Iqbal Choudhary:** Writing – review & editing, Supervision, Resources, Project administration.

Declaration of competing interest

The authors declare that they have no known competing financial interests or personal relationships that could have appeared to influence the work reported in this paper.

Acknowledgements

We acknowledge the generous help from Prof. Dr. Andrew P. Turnbull, Cancer Research Laboratories, UK. He very kindly provided the plasmid pETNHT-1, engineered with His-tagged USP7 catalytic domain.

Appendix A. Supplementary data

Supplementary data to this article can be found online at <https://doi.org/10.1016/j.heliyon.2024.e26345>.

References

- [1] R.B. Damgaard, *Cell Death Differ.* 28 (2) (2021) 423–426.
- [2] A. Ciechanover, A.L. Schwartz, *Biochim. Biophys. Acta Mol. Cell Res.* 1695 (1–3) (2004) 3–17.
- [3] N. Singh, A.B. Singh, *Crit. Rev. Oncol. Hematol.* 103 (2016) 22–26.
- [4] D. Komander, M.J. Clague, S. Urbé, *Nat. Rev. Mol. Cell Biol.* 10 (8) (2009) 550–563.
- [5] N.J. Schauer, X. Liu, R.S. Magin, L.M. Doherty, W.C. Chan, S.B. Ficarro, W. Hu, R.M. Roberts, R.E. Jacob, B. Stolte, A.O. Giacomelli, S. Perera, K. McKay, S. A. Boswell, E.L. Weisberg, A. Ray, D. Chauhan, S. Dhe-Paganon, K.C. Anderson, J.D. Griffin, J. Li, W.C. Hahn, P.K. Sorger, J.R. Engen, K. Stegmaier, J.A. Marto, S.J. Buhrlage, *Sci. Rep.* 10 (1) (2020) 1–15.
- [6] L. Nininahazwe, B. Liu, C. He, H. Zhang, Z.S. Chen, *Drug Discov. Today* 26 (2) (2021) 490–502.
- [7] Z. Wang, W. Kang, Y. You, J. Pang, H. Ren, Z. Suo, H. Liu, Y. Zheng, *Front. Pharmacol.* 10 (2019) 427.
- [8] S. Chen, Y. Liu, H. Zhou, *Int. J. Mol. Sci.* 22 (9) (2021) 4546.
- [9] A. Pozhidaeva, I. Bezsonova, *DNA Repair* 76 (2019) 30–39.
- [10] S. Pushpakom, F. Iorio, P.A. Eyers, K.J. Escott, S. Hopper, A. Wells, A. Doig, T. Williams, J. Latimer, C. McNamee, A. Norris, *Nat. Rev. Drug Discov.* 18 (1) (2019) 41–58.
- [11] A.P. Turnbull, S. Ioannidis, W.W. Krajewski, A. Pinto-Fernandez, C. Heride, A.C. Martin, L.M. Tonkin, E.C. Townsend, S.M. Buker, D.R. Lancia, J.A. Caravella, *Nature* 550 (7677) (2017) 481–486.
- [12] M. Mayer, B. Meyer, *J. Am. Chem. Soc.* 123 (2001) 6108–6117.
- [13] F.H. Niesen, H. Berglund, M. Vedadi, *Nat. Protoc.* 2 (2007) 2212–2221.
- [14] Min Hu, Pingwei Li, Muyang Li, Wenyu Li, Tingting Yao, Jia-Wei Wu, Wei Gu, Robert E. Cohen, Yigong Shi, *Cell* 7 (2002) 1041–1054.
- [15] K. Molland, Q. Zhou, A.D. Mesecar, *Acta Crystallogr. F: Structural Biology Communications* 70 (3) (2014) 283–287.
- [16] W.L. Jorgensen, D.S. Maxwell, Tirado-Rives, *J. Journal of the American Chemical Society* 118 (45) (1996) 11225–11236.
- [17] E. Harder, W. Damm, J. Maple, C. Wu, M. Reboul, J.Y. Xiang, L. Wang, D. Lupyran, M.K. Dahlgren, J.L. Knight, J.W. Kaus, *J. Chem. Theor. Comput.* 12 (1) (2016) 281–296.
- [18] Schrödinger Release 2020-2, LigPrep, Schrödinger, LLC, New York, NY, 2020.
- [19] T. Halgren, *J. Chem. Inf. Model.* 49 (2009) 377–389.
- [20] T. Halgren, *Chem. Biol. Drug Des.* 69 (2007) 146–148.
- [21] SiteMap, Schrödinger, LLC, New York, NY, 2020.
- [22] T.A. Halgren, R.B. Murphy, R.A. Friesner, H.S. Beard, L.L. Frye, W.T. Pollard, J.L. Banks, *J. Med. Chem.* 47 (7) (2004) 1750–1759.
- [23] R.A. Friesner, R.B. Murphy, M.P. Repasky, L.L. Frye, J.R. Greenwood, T.A. Halgren, P.C. Sanschagrin, D.T. Mainz, *J. Med. Chem.* 49 (21) (2006) 6177–6196.
- [24] K. Dimas, C. Demetzos, M. Marsellos, R. Sotiriadou, M. Malamas, D. Kokkinopoulos, *Planta Med.* 64 (3) (1998) 208–211.
- [25] S. Javaid, M. Shaikh, N. Fatima, M.I. Choudhary, *PLoS One* 14 (2019) e0225056.
- [26] S. Javaid, H. Zafar, Atia-tul-Wahab, V. Gervais, P. Ramos, I. Muller, A. Milon, Atta-ur-Rahman, M.I. Choudhary, *Bioorg. Chem.* 114 (2021), 105021–105021.
- [27] T. An, Y. Gong, X. Li, L. Kong, P. Ma, L. Gong, H. Zhu, C. Yu, J. Liu, H. Zhou, B. Mao, *Biochem. Pharmacol.* 131 (2017) 29–39.
- [28] D.C. Rio, M. Ares, G.J. Hannon, T.W. Nilsen, 2010, Cold Spring Harb. Protoc. (6) (2010). pdb-prot5439.
- [29] T.D. Claridge, *High-resolution NMR Techniques in Organic Chemistry*, vol. 27, Elsevier, 2016.
- [30] Jenny L. Hall, A. Sohail, E.J. Cabrita, C. Macdonald, T. Stockner, H.H. Sitte, J. Angulo, F. MacMillan, *Sci. Rep.* 10 (1) (2020) 1–9.

- [31] W. Samuel, S. Monaco, R. Nepravishta, J. Angulo, *Methods in Enzymology*, vol. 615, Academic Press, 2019, pp. 423–451.
- [32] C. Wang, Y. Cao, X. Chen, M. Cai, W. Huang, *Medicine* 99 (49) (2020).
- [33] K. Kyuki, T. Shibuya, K. Tsurumi, H. Fujimura, *Jpn. J. Pharmacol.* 33 (1) (1983) 121–132.
- [34] T.G. Kantor, *Pharmacotherapy* 6 (3) (1986) 93–102.
- [35] E.P. MacCarthy, S.S. Bloomfield, *Pharmacotherapy* 3 (4) (1983) 193–217.
- [36] S. Hunskaar, D. Donnell, *J. Int. Med. Res.* 19 (2) (1991) 71–87.
- [37] Y.E. Yarker, K.L. Goa, A. Fitton, *Oxybutynin*, *Drugs Aging* 6 (3) (1995) 243–262.
- [38] A. El Hefny, A. El Beshlawy, S. Nour, M. Said, *J. Int. Med. Res.* 14 (5) (1986) 267–273.
- [39] M.K. Ito, A.R. Smith, M.L. Lee, *Clin. Pharm.* 11 (7) (1992) 603–617.
- [40] E. Dinnerstein, B.C. Jobst, P.D. Williamson, *Arch. Neurol.* 64 (9) (2007) 1344–1346.
- [41] S. Mathews, A. Reid, C. Tian, Q. Cai, *Clin. Exp. Gastroenterol.* 3 (2010) 11.
- [42] G. Li, Y. Shen, J. Luo, H. Li, *Medicine* 96 (39) (2017) e8142.
- [43] C. Airoidi, S. Merlo, E. Sironi, *Bentham Science Publishers* (2015) 147–219.
- [44] M.C. Lo, A. Aulabaugh, G. Jin, R. Cowling, J. Bard, M. Malamas, G. Ellestad, *Anal. Biochem.* 332 (1) (2004) 153–159.
- [45] I. Lamberto, X. Liu, H.S. Seo, N.J. Schauer, R.E. Jacob, W. Hu, D. Das, T. Mikhailova, E.L. Weisberg, J.R. Engen, K.C. Anderson, D. Chauhan, S. Dhe-Paganon, S. J. Buhrlage, *Cell Chem. Biol.* 24 (12) (2017) 1490–1500.
- [46] Y. Sheng, V. Saridakis, F. Sarkari, S. Duan, T. Wu, C.H. Arrowsmith, L. Frappier, *Nat. Struct. Mol. Biol.* 13 (3) (2006) 285–291.
- [47] Dale S. Haines, *Leuk. Lymphoma* 26 (3–4) (1997) 227–238.
- [48] P. Sonal, A. Alam, R. Pant, S. Chattopadhyay, *Front. Immunol.* 10 (2019) 2872.
- [49] H. Yi-Heng, M.C. Lafita-Navarro, L. Zacharias, N. Borenstein-Auerbach, M. Kim, S. Barnes, J. Kim, J. Shay, R.J. DeBerardinis, M. Conacci-Sorrell, *Cell Commun. Signal.* 17 (1) (2019) 1–16.
- [50] Q. Xiao, J. Werner, N. Venkatachalam, K.E. Boonekamp, M.P. Ebert, T. Zhan, *Biomolecules* 12 (3) (2022) 453.
- [51] Si-Min Qi, Gang Cheng, Xiang-Dong Cheng, Zhiyuan Xu, Beihua Xu, Wei-Dong Zhang, Jiang-Jiang Qin, *Front. Cell Dev. Biol.* 8 (2020) 233.
- [52] J. Liu, C.T. Leung, L. Liang, Y. Wang, J. Chen, K.P. Lai, W.K.F. Tse, *Cancers* 14 (14) (2022) 3547.
- [53] L. Novellasdemunt, F. Valentina, C. Laura, A. Pedro, K. Anna, E. Vesela, P.S. Ambrosius, SW Li Vivian, *Cell Rep.* 21 (3) (2017) 612–627.
- [54] X. Li, K. Lingmei, Y. Qihong, D. Aizhu, J. Xiaoman, C. Bicheng, C. Lin, A. Tao, L. Yan, *J. Biol. Chem.* 295 (11) (2020) 3576–3589.
- [55] O. Carugo, S. Pongor, *Protein Sci.* 10 (7) (2001) 1470–1473.